ELSEVIER

Coordination Chemistry Reviews
200–202 (2000) 105–129

COORDINATION CHEMISTRY REVIEWS

www.elsevier.com/locate/ccr

Bimetallic dioxygen complexes derived from 'end-off' compartmental ligands

Masatatsu Suzuki [a,*], Hideki Furutachi [a], Hisashi Ōkawa [b,1]

[a] *Department of Chemistry, Faculty of Science, Kanazawa University, Kakuma-machi, Kanazawa 920-1192, Japan*

[b] *Department of Chemistry, Graduate School of Science, Kyushu University, Hakozaki, Higasiku, Fukuoka 812-8581, Japan*

Received 9 November 1999; accepted 23 February 2000

Contents

Abstract

This article deals with recent progress in bimetallic dioxygen complexes derived from 'end-off' compartmental ligands having a phenolic or alcoholic oxygen as the endogenous bridge. Focus is placed on oxygenation of μ-phenoxo and μ-alkoxo bridged dimetal(II)

* Corresponding author. Tel.: +81-76-2645701; fax: +81-76-2645742.

[1] Also corresponding author. Tel.: +81-92-6422596; fax: +81-92-6322734.

E-mail addresses: suzuki@cacheibm.s.kanazawa-u.ac.jp (M. Suzuki), okawascc@mbox.nc.kyushu-u.ac.jp (H. Ōkawa).

PII: S0010-8545(00)00323-4

complexes (metal(II) = Co(II), Fe(II), and Cu(II)) in view of the electronic and stereochemical nature of the compartmental ligands and bimetallic core structures.

Keywords: Dioxygen complexes; Compartmental ligands; Thermodynamics; Reactivity

1. Introduction

Bimetallic cores are versatile at the active sites of many metalloenzymes and model studies using simple dinuclear metal complexes are becoming increasingly important to understand the biological significance of such bimetallic cores. For this purpose dinucleating compartmental ligands of 'end-off' type', 'side-off' type, and 'macrocyclic' type have been developed [1–7].

In particular, compartmental ligands of the 'end-off' type, having a phenolic or alcoholic oxygen as endogenous bridge, have often been used for modeling bimetallic biosites, because they provide μ-phenoxo-μ-carboxylato- and μ-phenoxo-di(μ-carboxylato)dimetal cores (or analogous μ-alkoxo-bridged cores) relevant to the active sites of some bimetallic enzymes. An important function of bimetallic biosites is seen in dioxygen transport by hemocyanin (2Cu) [8] and hemerythrin (2Fe) [9], and dioxygen activation by tyrosinase (2Cu) [10] and methane monooxygenase (2Fe) [11]. The present review is concerned with bimetallic dioxygen complexes derived from the phenol- and alcohol-based compartmental ligands (Fig. 1), to understand fundamental factors contributing to the stability and/or reactivity of the dioxygen complexes.

2. Dicobalt dioxygen complexes

Dicobalt-dioxygen (peroxo or superoxo) complexes have been extensively studied [12–14]. Most μ-peroxo complexes reported so far have been synthesized by oxygenation of monomeric cobalt(II) precursor complexes. Recently, 'end-off' compartmental ligands having an alkoxo or phenoxo bridging group (Fig. 2) were used to produce μ-peroxo dicobalt(III) complexes. The ligands form μ-phenoxo-μ-carboxylato- and μ-alkoxo-μ-carboxylatodicobalt(II) complexes, $[Co_2(L)(O_2CR)]^{2+}$, where each cobalt(II) center has a five coordinate geometry [15–19].

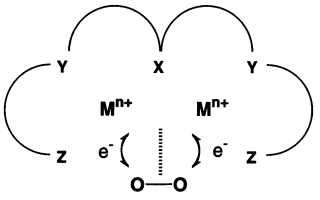

Fig. 1. Juxtapositional dioxygen binding to a bimetallic center organized by an 'end-off' compartmental ligand.

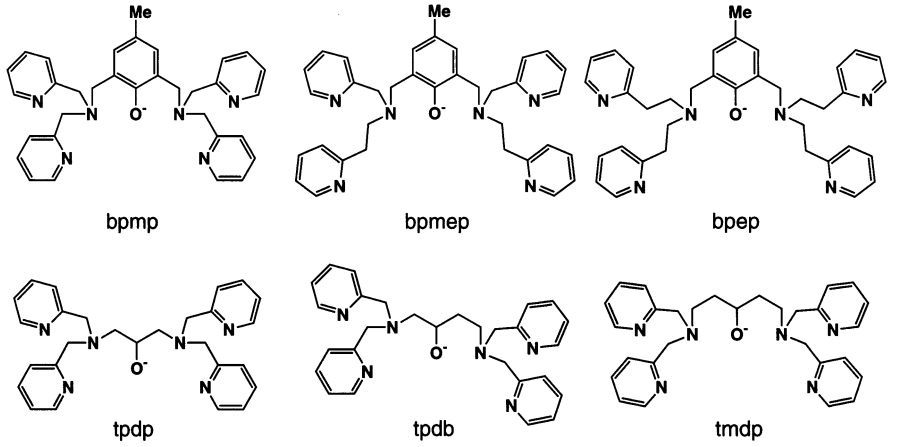

Fig. 2. 'End-off' compartmental ligands for dicobalt complexes.

All the $[Co_2(L)(O_2CR)]^{2+}$ complexes except for the bpep complex react with O_2 to generate brown-colored μ-peroxo complexes. $[Co_2(bpmp)(O_2CC_6H_5)]^{2+}$ (**1**-$O_2CC_6H_5$) is oxygenated in acetonitrile at ambient temperature and reversibly deoxygenated by purging the solution with N_2 at boiling temperature. This oxygenation–deoxygenation cycle can be repeated many times. In contrast, a di(μ-acetato)dicobalt(II) complex of bpmp, $[Co_2(bpmp)(O_2CCH_3)_2]^{2+}$ (**2**), does not react with O_2 in acetonitrile, probably because each Co is in a six-coordinate environment and has no vacant site for O_2 binding. On the other hand, in MeOH **2** gradually reacts with O_2 to generate a peroxo species, indicating that one of the carboxylato bridges is dissociated in MeOH to produce **1**-O_2CCH_3.

The structures of two μ-peroxo complexes, $[Co_2(\mu\text{-}O_2)(bpmp)(O_2CC_6H_5)]^{2+}$ (oxy-**1**-$O_2CC_6H_5$) [15] and $[Co_2(\mu\text{-}O_2)(tpdb)(O_2CCH_3)]^{2+}$ (oxy-**6**-O_2CCH_3) [18], have been reported (Fig. 3). In both complexes, two cobalt(III) ions are triply bridged by the phenoxo or alkoxo oxygen of ligand, one carboxylato group, and one peroxo group. The peroxo group assumes a *cis*-μ-1,2 bridging mode. The O–O bond distances for oxy-**1**-$O_2CC_6H_5$ and oxy-**6**-O_2CCH_3 are 1.43 and 1.38 Å, respectively, that are characteristic of peroxo cobalt(III) complexes. The ν(O–O) Raman band observed at 830 cm^{-1} for oxy-**1**-$O_2CC_6H_5$ is consistent with the peroxo formulation [20].

The Dioxygen affinity of the phenoxo bridged complexes, $[Co_2(L)(O_2CCH_3)]^{2+}$ (L = bpmp (**1**-O_2CCH_3), bpmep (**3**-O_2CCH_3), and bpep (**4**-O_2CCH_3)), is dependent on the nature of the side arms of the dinucleating ligands [16]. Introduction of the 2-pyridylethyl side arm significantly lowers the dioxygen affinity; the $P(O_2)_{1/2}$ values of **1**-O_2CCH_3 and **3**-O_2CCH_3 in acetonitrile at 20°C are < 0.1 and 24 Torr, respectively, where $P(O_2)_{1/2}$ represents the dioxygen partial pressure at which half the amount of complex is oxygenated:

$$[Co_2] + O_2 \overset{K}{\rightleftharpoons} [Co_2(\mu\text{-}O_2)] \quad K = [Co_2(\mu\text{-}O_2)]/[Co_2] \cdot P(O_2) = 1/P(O_2)_{1/2}$$

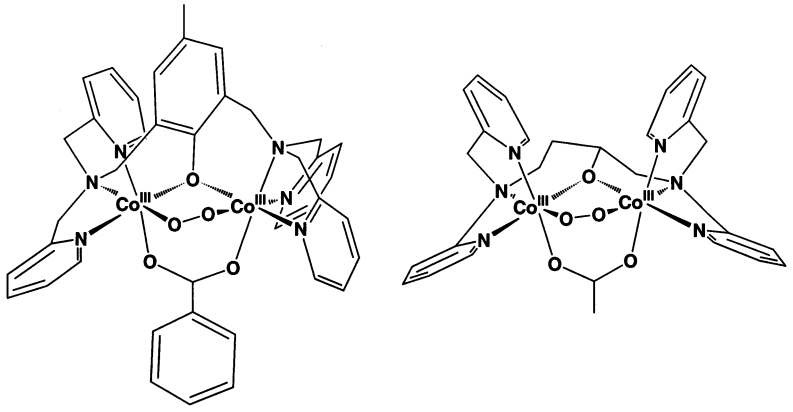

Fig. 3. Structures of μ-peroxo dicobalt(III) complexes, $[Co_2(\mu\text{-}O_2)(bpmp)(O_2CC_6H_5)]^{2+}$ (oxy-**1**-$O_2CC_6H_5$) and $[Co_2(\mu\text{-}O_2)(tpdb)(O_2CCH_3)]^{2+}$ (oxy-**6**-O_2CCH_3).

Complex **4**-O_2CCH_3 has no reactivity toward O_2 even at -40°C. Evidently, the dinuclear core of **4**-O_2CCH_3 is unfavorable for a *cis*-μ-1,2-peroxo formation.

The dioxygen affinity of dicobalt(II) complexes and the thermal stability of the resulting peroxo complexes against irreversible oxidation are influenced by the condensed chelate rings associated with the bridging oxygen and two articular ligand nitrogen atoms [17,18]. The dioxygen affinity of $[Co_2(L)(O_2CCH_3)]^{2+}$ (L = bpmp (**1**-O_2CCH_3), tmdp (**5**-O_2CCH_3), tpdb (**6**-O_2CCH_3), tpdp (**7**-O_2CCH_3)) decreases in the order: **1**-O_2CCH_3 (< 0.1 Torr at 20°C) > **5**-O_2CCH_3 (ca. 3 Torr at 20°C) > **6**-O_2CCH_3 (ca. 720 Torr at 20°C) > **7**-O_2CCH_3 (ca. 780 Torr at -15.6°C). The order is correlated with the chelate ring size in the bridging skeleton; **1**-O_2CCH_3 and **5**-O_2CCH_3 each have [6-6] condensed chelate rings, **6**-O_2CCH_3 has [5-6] chelate rings and **7**-O_2CCH_3 has [5-5] chelate rings.

The thermal stability of the μ-peroxo complexes against irreversible oxidation is also dependent on the nature of the dinucleating ligands. The μ-peroxo complexes of **5**-O_2CCH_3 and **6**-O_2CCH_3 (with alkoxo bridge) are thermally less stable than the μ-peroxo complex of **1**-O_2CCH_3 (with phenoxo bridge) against irreversible oxidation. This is probably due to the strong electron-donating ability of the alkoxo bridge compared with the phenoxo bridge. A mixed-valence dicobalt(II,III) complex, $[Co^{II}Co^{III}(tpdb)(O_2CCH_3)_2]^{2+}$, was obtained by irreversible oxidation of **6**-O_2CCH_3 [18]. The asymmetric nature of the tpdb ligand probably leads to a stabilization of the mixed-valence state. An analogous mixed-valence diiron(II,III) complex, $[Fe^{II}Fe^{III}(tpdb)(O_2CC_6H_5)_2]^{2+}$, was also derived from the oxidation of $[Fe^{II}_2(tpdb)(O_2CC_6H_5)_2]^{2+}$ with O_2 [21].

The peroxo complexes $[Co_2(\mu\text{-}O_2)(L)(O_2CCH_3)]^{2+}$ (L = tmdp (oxy-**5**-O_2CCH_3), tpdb (oxy-**6**-O_2CCH_3), or tpdp (oxy-**7**-O_2CCH_3)) are electrochemically oxidized to generate stable superoxo complexes $[Co_2(\mu\text{-}O_2)(L)(O_2CCH_3)]^{3+}$ [17,18].

$$[Co_2(\mu\text{-}O_2)(L)(O_2CCH_3)]^{2+} \rightarrow [Co_2(\mu\text{-}O_2)(L)(O_2CCH_3)]^{3+} + e^-$$

The superoxo complexes show EPR signals with a small anisotropy ($g_{\|} = 2.07$ and $g_{\perp} = 1.99$) at liquid nitrogen temperature. The appearance of 15 hyperfine lines ($A = 20$ gauss) in the $g_{\|}$ region indicates that an unpaired-electron is mainly localized on O_2^- moiety and weakly coupled with two equivalent ^{59}Co nuclei (Co^{3+}–O_2^-–Co^{3+}).

3. Diiron dioxygen complexes

It is generally known that iron–dioxygen complexes are highly susceptible to irreversible oxidation even at low temperature. For this reason, μ-peroxo diiron complexes are very limited [19,22–28], and only three peroxo complexes have so far been crystallographically characterized [26–28]. In order to suppress irreversible oxidation of μ-peroxo diiron(III) complexes, modulations of 'end-off' compartmental ligands are made so as to provide geometrical preference for stabilizing μ-peroxo diiron complex. μ-Peroxo diiron complexes can be obtained by two methods: (1) the oxygenation of diiron(II) complexes; and (2) the reaction of iron(III) complexes with H_2O_2. In earlier work, the latter method was adopted to provide μ-peroxo diiron(III) complexes.

$$Fe_2^{II}(L) + O_2 \rightleftharpoons Fe_2^{III}(\mu\text{-}O_2)(L)$$

$$Fe_2^{III}(L)(X)_2 + H_2O_2 \rightarrow Fe_2^{III}(\mu\text{-}O_2)(L) + 2HX$$

3.1. μ-Peroxo diiron(III) complexes from diiron(III) complexes and H_2O_2

Nishida et al. found that a diiron(III) complex of hptb (Fig. 4), $Fe_2(hptb)(NO_3)_5 \cdot 4CH_3OH$, produces an intensely green species with λ_{max} at 600 nm ($\varepsilon = 1300\ M^{-1}\ cm^{-1}$) upon reaction with H_2O_2 in MeOH and DMF [29,30]. It showed a ν(O–O) Raman band at 890 cm^{-1}, indicating the formation of a μ-peroxo diiron(III) complex. Later, Que et al. characterized the diiron(III) complex as $[Fe_2(hptb)(OH)(NO_3)_2](NO_3)_2 \cdot MeOH$ (**8**) and studied its green H_2O_2-reaction product (oxy-**8**) by various physicochemical techniques including EXAFS and

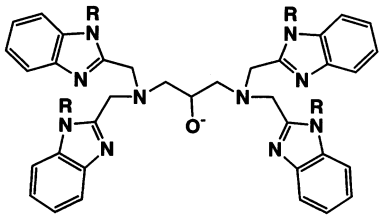

Fig. 4. Chemical structure of hptb and *N*-Et-hptb.

resonance Raman spectroscopy [31]. The intense absorption band observed at 560–600 nm depending upon the solvent used, is assigned to the peroxo(π*)-to-Fe(III) LMCT transition.

A diiron(III) complex $[Fe_2(5\text{-Me-HXTA})(O_2CCH_3)_2]^-$ (**9**) (Fig. 5) also reacts with H_2O_2 to produce a μ-peroxo diiron(III) species [32]. The complex has a carboxylate-rich coordination environment about each metal. The addition of H_2O_2 to **9** causes the substitution of one bridging acetate group for O_2^{2-} to produce the μ-peroxo species (oxy-**9**), which shows a ν(O–O) Raman feature at 884 cm^{-1} and a peroxo-to-Fe(III) LMCT band at 470 nm. The LMCT band is significantly higher in energy than those of the peroxo complexes having a nitrogen-rich coordination environment (550–800 nm). The high energy shift of the LMCT transition band for oxy-**9** is attributable to a decrease in Lewis acidity of the iron centers (lifting of the d-orbitals), due to a strong electron-donating ability of carboxylato group relative to the nitrogen base.

3.2. μ-Peroxo diiron(III) complexes by oxygenation of diiron(II) complexes

Three important factors are taken into consideration to obtain the μ-peroxo complexes by oxygenation of diiron(II) complexes: (1) coordinatively-unsaturated five-coordination about each iron(II) center to provide a vacant site for O_2 binding; (2) a sterically-hindered environment and/or hydrophobic cavity around the O_2 binding site to protect the coordinated peroxo ligand from some unfavorable decay reactions; and (3) weak-electron-donation from ligand to Fe(II) so as to stabilize iron(II) oxidation state to achieve a reversible oxygenation–deoxygenation process. For this purpose the 'end-off' compartmental ligands of Fig. 6 have been developed.

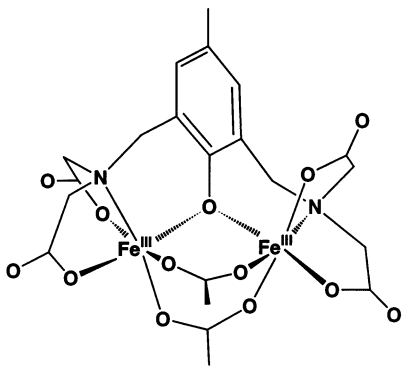

$[Fe_2(5\text{-Me-HXTA})(O_2CCH_3)_2]^-$ (**9**)

Fig. 5. Structure of diiron(III) complex $[Fe_2(5\text{-Me-HXTA})(O_2CCH_3)_2]^-$ (**9**).

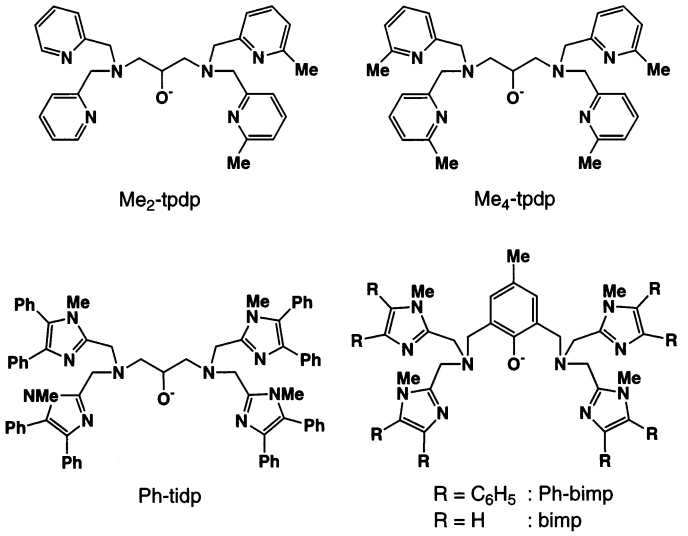

Fig. 6. 'End-off' compartmental ligands for diiron complexes.

3.2.1. Diiron(II) complexes

Que et al. synthesized a diiron(II) complex, $[Fe_2(N\text{-Et-hptb})(O_2CC_6H_5)]^{2+}$ (**10**-$O_2CC_6H_5$), of a hptb derivative described above [24]. The complex consists of two five-coordinate iron centers with an N_3O_2 donor set (Fig. 7) and reacts with O_2 in CH_2Cl_2 at -60°C to give $[Fe_2(\mu\text{-}O_2)(N\text{-Et-hptb})(O_2CC_6H_5)]^{2+}$ (oxy-**10**-$O_2CC_6H_5$).

The dinucleating ligands in Fig. 6 similarly form diiron(II) complexes of the general formula $[Fe_2(L)(O_2CR)]^{2+}$, often as aqua adducts $[Fe_2(L)(O_2CR)(H_2O)_n]^{2+}$ [25]. For example, Me_4-tpdp forms an aqua complex, $[Fe_2(Me_4\text{-tpdp})(O_2CC_6H_5)(H_2O)]^{2+}$ (**11**-$O_2CC_6H_5$), which has distinct five- and six-coordinate environments about the two iron centers (Fig. 7). The reflectance spectrum of **11**-$O_2CC_6H_5$ shows three d-d bands at 12 400, ca. 8000 (shoulder), and ca. 6000 cm^{-1} (Table 1). The bands at 12 400 and ca. 6000 cm^{-1} can be assigned to the five-coordinate iron(II) center and the bands at 12 400 and ca. 8000 cm^{-1} (shoulder) to the six-coordinate iron(II) center. In CH_2Cl_2, dissociation of the coordinated water occurs and the electronic spectrum displays two absorption bands at 11 850 ($\varepsilon = 30$) and ca. 5800 cm^{-1} (ε = ca. 70 M^{-1} cm^{-1}). Similarly, $[Fe_2(Ph\text{-bimp})(O_2CC_6H_5)(H_2O)]^{2+}$ (**13**-$O_2CC_6H_5$) shows three d-d bands as a powder but two bands in CH_2Cl_2 solution [26,33]. The presence of two five-coordinate iron centers is essential for O_2 binding. The di(carboxylato) diiron(II) complexes, $[Fe_2(L)(O_2CR)_2]^{+}$ (L = bpmp [34], bzimp [35] and Ph-bimp [36]), react irreversibly with O_2 to produce mixed-valence diiron(II,III) complexes $[Fe_2(L)(O_2CR)_2]^{2+}$. It must be mentioned that each metal of $[Fe_2(L)(O_2CR)_2]^{2+}$ has a six-coordinate environment.

The structural features of $[Fe_2(N\text{-Et-hptb})(O_2CC_6H_5)]^{2+}$ (**10**-$O_2CC_6H_5$), $[Fe_2(Me_4\text{-tpdp})(O_2CC_6H_5)(H_2O)]^{2+}$ (**11**-$O_2CC_6H_5$), and $[Fe_2(Ph\text{-tidp})(O_2CC_6H_5)]^{2+}$

Table 1
Structural, electrochemical, and visible spectral data for diiron(II) complexes

Complex	Fe···Fe (Å)	Av. Fe–N_{arom} (Å)	Av. Fe–N_{all} (Å)	Av. Fe–O_{alkoxo}	$E_{1/2}$(II,III/II,II)[c]	$\tilde{\nu}_{max}$ (cm^{-1}) (ε (M^{-1} cm^{-1}))[c]	Refs.
10-$O_2CC_6H_5$	3.473(7)	2.07	2.15	1.97			[24]
11-$O_2CC_6H_5$	3.684(1)	2.19[a], 2.31[b]	2.19[a], 2.27[b]	2.02	605 (490)[d]	11 850 (30), ca. 5800 (ca. 70)12 400[e], ca. 8000[e,f], ca. 6000[e]	[25]
11-O_2CCF_3					750 (640)[d]		[25]
12-$O_2CC_2H_5$					445		[19]
12-$O_2CC_6H_5$	3.592(1)	2.12	2.19	2.00	460 (345)[d]	11 140 (50), ca. 5780 (ca. 100)	[19]
12-$O_2CC_6F_5$					505	11 110 (54), ca. 5850 (ca. 73)	[19]
12-O_2CCF_3					605 (420)[d]	10 870 (31), ca. 5880 (ca. 73)	[19]
14-O_2CCF_3							[19]

[a] Five-coordinate center.
[b] Six-coordinate center.
[c] In CH_2Cl_2.
[d] In CH_3CN.
[e] Reflectance spectrum.
[f] Shoulder.

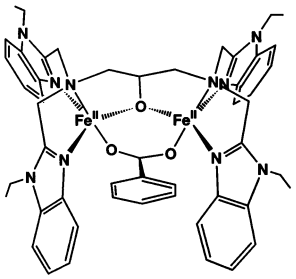

$[Fe_2(N\text{-Et-hptb})(O_2CC_6H_5)]^{2+}$
(**10**-$O_2CC_6H_5$)

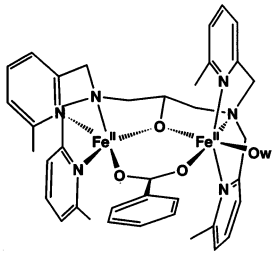

$[Fe_2(Me_4\text{-tpdp})(O_2CC_6H_5)(H_2O)]^{2+}$
(**11**-$O_2CC_6H_5$)

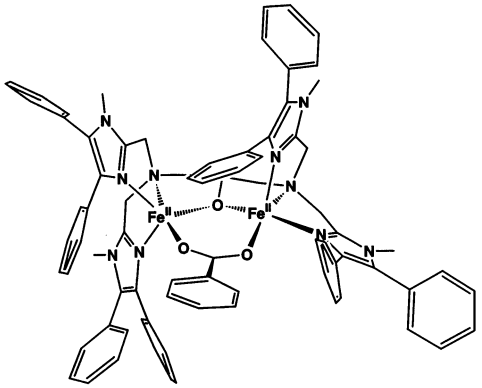

$[Fe_2(Ph\text{-tidp})(O_2CC_6H_5)]^{2+}$
(**12**-$O_2CC_6H_5$)

Fig. 7. Structures of diiron(II) complexes, $[Fe_2(N\text{-Et-hptb})(O_2CC_6H_5)]^{2+}$ (**10**-$O_2CC_6H_5$), $[Fe_2(Me_4\text{-tpdp})(O_2CC_6H_5)(H_2O)]^{2+}$ (**11**-$O_2CC_6H_5$), and $[Fe_2(Ph\text{-tidp})(O_2CC_6H_5)]^{2+}$ (**12**-$O_2CC_6H_5$).

(**12**-$O_2CC_6H_5$) are summarized in Table 1. Introduction of a methyl group into the six-position of the pyridyl group in **11**-$O_2CC_6H_5$ and phenyl groups into the four and five-positions of the imidazole group in **12**-$O_2CC_6H_5$ has significant influence on the Fe–N bond distances of the complexes. The average Fe–N(pyridine) bond distances for the five- and six-coordinate iron centers of **11**-$O_2CC_6H_5$ are 2.19 and 2.31 Å [25], respectively, and the average Fe–N(imidazole) bond distance of **12**-$O_2CC_6H_5$ is 2.12 Å [19]. Those Fe–N bond distances are substantially longer than the Fe–N(benzimidazole) bond distances of **10**-$O_2CC_6H_5$ (2.07 Å) [24]. The elongation of the Fe–N bonds naturally arises from steric crowding of the methyl or phenyl groups introduced into the side arm. Such elongation of the Fe–N bonds weakens the electron-donating ability of the nitrogen donors, stabilizing the iron(II) oxidation state and hence leading to facilitating a reversible oxygenation–deoxygenation process.

Table 2
Raman, Mössbauer, and visible spectral data for μ-peroxo diiron(III) complexes

Complex	ν(O–O) (Δ^{18}O)	$\delta(\Delta E)$ (mm s^{-1})	λ_{max} (nm) (ε (M^{-1} cm^{-1}))	Refs.
oxy-**9**	884		480 (2370)	[32]
oxy-**10**-$O_2CC_6H_5$	900 (−50)	0.52 (0.72)	588 (1500)	[24]
oxy-**11**-$O_2CC_6H_5$	918, 891 (−47)		616 (ca. 2000)	[25]
16	900 (−50)			[27]
oxy-**13**-$O_2CC_6H_5$		0.58 (0.74)	ca. 800 (ca. 1700)	[26]
		0.65 (1.70)		
17	888 (−46)	0.66 (1.40)	694 (2650)	[28]
$[Fe_2O(O_2)(L)_2]^{2+}$ [a]	848 (−46)	0.54 (1.68)	648 (1200)	[37]
oxy-Hr	844 (−47)	0.48 (1.03)	500 (2200)	[38]
		0.49 (1.90)		
MMOH-P		0.66 (1.51)	600–650 (1500)	[39,40]
RNR R2	870 (−46)[c]	0.63 (1.58)[d]	700 (ca. 1500)[d]	[41,42]
Δ9D[b]	898 (−53)		700	[43]

[a] L = tris(6-methyl-2-pyridylmethyl)amine.
[b] Stearoyl-ACP Δ^9-desaturase.
[c] W48F/D84E.
[d] D84E.

The $E_{1/2}$ values for Fe_2(II,II)/Fe_2(II,III) redox couple measured by cyclic voltammetry are useful to estimate the electron-donating ability of dinucleating ligands. The $E_{1/2}$ values for $[Fe_2(Me_2\text{-tpdp})(O_2CCF_3)]^{2+}$ (**14**-O_2CCF_3) and **11**-O_2CCF_3 are 420 and 640 mV versus SCE, respectively, in acetonitrile (Table 1) [19,25]. Thus, the introduction of a methyl group into the pyridyl residue causes a significant positive shift of the $E_{1/2}$ value, in harmony with the elongation of the Fe–N bonds. The $E_{1/2}$ values for **11**-$O_2CC_6H_5$ and **12**-$O_2CC_6H_5$ are 490 and 345 mV versus SCE, respectively, indicating that electron-donating ability decreases in the order: Me_2-tpdp, Ph-tidp > Me_4-tpdp [19,25]. $E_{1/2}$ values of diiron(II) complexes can be modulated by the bridging carboxylato group. For example, the $E_{1/2}$ values for **12**-O_2CR decrease in the order $R = CF_3 > C_6F_5 > C_6H_5 > C_2H_5$.

3.2.2. Thermal stability and reversibility of μ-peroxo diiron(III) complexes

Complexes **11**–**14** react with O_2 to give μ-peroxo complexes with a color change from almost colorless to deep blue or deep green. The moderately intense band at 550–800 nm ($\varepsilon = 1000$–3000 M^{-1} cm^{-1}) observed for the peroxo complexes is attributable to the peroxo(π*)-to-Fe(III) LMCT transition [19,25,26]. Raman, Mössbauer, and visible spectral data for the μ-peroxo complexes are given in Table 2.

The thermal stability of the μ-peroxo complexes against irreversible oxidation and the oxygenation–deoxygenation reversibility are highly dependent upon the nature of the dinucleating ligands. The reaction of $[Fe_2(tpdp)(O_2CC_6H_5)]^{2+}$ (**15**-$O_2CC_6H_5$) with O_2 at −40°C in acetonitrile resulted in an instantaneous irre-

versible oxidation. Irreversible oxidation of **15**-$O_2CC_6H_5$ was also observed in CH_2Cl_2 even at -80°C, though a μ-peroxo species was detected in a CH_2Cl_2–DMSO solution [24b]. $[Fe_2(Me_2\text{-tpdp})(O_2CCF_3)]^{2+}$ (**14**-O_2CCF_3) in acetone at -60°C produced a μ-peroxo species, which gradually decomposed within a few hours. Thus, the oxygenation of **14**-O_2CCF_3 is not reversible. $[Fe_2(Me_4\text{-tpdp})(O_2CC_6H_5)(H_2O)]^{2+}$ (**11**-$O_2CC_6H_5$), and $[Fe_2(Me_4\text{-tpdp})(O_2CCF_3)(H_2O)_2]^{2+}$ (**11**-O_2CCF_3) show a reversible oxygenation in CH_2Cl_2 below -40°C. The resulting μ-peroxo species are reasonably stable and can be deoxygenated by bubbling Ar into the solution. At ambient temperature, the μ-peroxo complexes irreversibly oxidized to give brown colored species. $[Fe_2(Ph\text{-tidp})(O_2CR)]^{2+}$ (**12**-$O_2CC_6H_5$, **12**-$O_2CC_6F_5$, and **12**-O_2CCF_3) also produce μ-peroxo species below -40°C. The μ-peroxo complexes are deoxygenated by warming up to room temperature without serious irreversible oxidation, although the $[Fe_2(Ph\text{-tidp})(O_2CR)]^{2+}$ complexes were gradually oxidized under an O_2 atmosphere at room temperature. Thus, the Ph-tidp μ-peroxo complexes are thermally more stable than the Me_4-tpdp complexes. $[Fe_2(Ph\text{-bimp})(O_2CC_6H_5)(H_2O)]^{2+}$ (**13**-$O_2CC_6H_5$) forms $[Fe_2(\mu\text{-}O_2)(Ph\text{-bimp})(O_2CC_6H_5)]^{2+}$ (oxy-**13**-$O_2CC_6H_5$) ($\lambda_{max} = 500–800$ nm (ε = ca. 1700 M^{-1} cm^{-1})) in acetonitrile at 20°C. Oxy-**13**-$O_2CC_6H_5$ is stable for several hours and is deoxygenated by boiling the acetonitrile solution under N_2. The oxygenation at 20°C and the deoxygenation by boiling the solution can be repeated several times. Thus, the oxygenation is reversible at 20°C and oxy-**13**-$O_2CC_6H_5$ is substantially stable against irreversible oxidation compared with the μ-peroxo complexes mentioned above. The relative thermal stability of the μ-peroxo complexes decreases in the order of the dinucleating ligands: Ph-bimp > Ph-tidp > Me_4-tpdp > Me_2-tpdp > tpdp. Evidently, the introduction of a bulky substituent into the pyridyl or imidazole residue suppresses some deleterious, irreversible decay reactions of the μ-peroxo species.

The thermal stability of μ-peroxo complexes is also dependent upon the nature of bridging carboxylates; kinetic studies for the decomposition of $[Fe_2(\mu\text{-}O_2)(N\text{-Et-hptb})(O_2CC_6H_4\text{–X})]^{2+}$ (oxy-**10**-$O_2CC_6H_4$–X) indicate that an electron-donating ring-substituent (X) accelerates the decay reaction [27]. It is found that $[Fe_2(\mu\text{-}O_2)(N\text{-Et-hptb})(OPPh_3)_2]^{3+}$ (**16**) is thermally more stable than oxy-**10**-$O_2CC_6H_5$ [27]. The high thermal stability of **16** is explained by the weak electron-donating ability of $OPPh_3$ relative to benzoate.

There is a disagreement about the decomposition mechanism of the μ-peroxo diiron(III) complexes. Dong et al. reported a first-order decomposition process for oxy-**10**-$O_2CC_6H_4$-X and proposed that the thermal decomposition process involves a diiron(IV) species produced by homolytic cleavage of the O–O bond shown in Scheme 1(a) [27]. Feig et al. observed a second-order decomposition process for oxy-**10**-$O_2CC_6H_5$, oxy-**11**-$O_2CC_6H_5$, and oxy-**15**-$O_2CC_6H_5$ and proposed bimolecular decomposition pathways through the formation of tetranuclear species in the transition state (Scheme 1(b)) [44]. A similar bimolecular decomposition pathway involving a tetranuclear mixed valence (μ_4-peroxo)tetrairon(II,II,III,IV) species in the transition state has also been proposed for the reaction of dioxygen with carboxylate-bridged diiron(II) complexes (Scheme 1(c)) [45]. Further complicated decomposition pathways have been also suggested [46,47].

If the decay reaction proceeds via a high-valent species such as Fe(IV), a strong electron donor may facilitate the formation of an Fe(IV) species and hence the decomposition of the μ-peroxo diferric species (Scheme 1(a)). If the decay reaction occurs through bimolecular processes such as the disproportionation of the peroxo ligands (Scheme 1(b)), reduction of the peroxo ligand by a diiron(II) species (Scheme 1(c)), and the substitution of the peroxo ligand for solvent molecules and/or hydroxide ion present as an impurity (Scheme 1(d)), the steric nature of the ligand must be important; a sterically bulky ligand providing a hydrophobic surrounding about the μ-peroxo group may suppress such unfavorable decay reactions. In either case, a bulky substituent would suppress the irreversible oxidation and facilitate the reversible oxygenation–deoxygenation process.

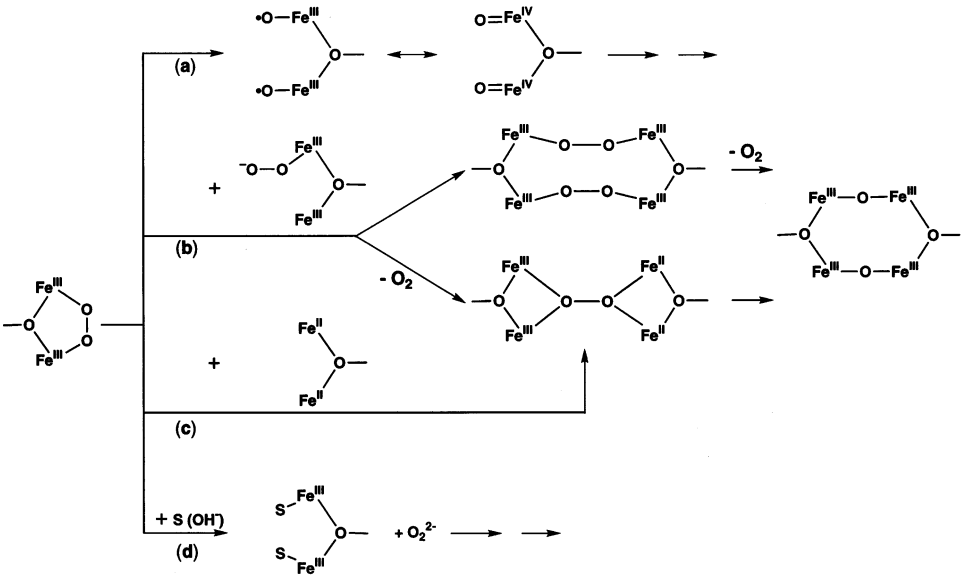

Scheme 1. Possible decomposition processes of μ-peroxo diiron(III) complexes.

3.2.3. Structures of μ-peroxo diiron(III) complexes

The crystal structures of three μ-peroxo diiron complexes, $[Fe_2(\mu\text{-}O_2)(N\text{-Et-hptb})(OPPh_3)_2]^{3+}$ (**16**) [27], $[Fe_2(\mu\text{-}O_2)(Ph\text{-bimp})(O_2CC_6H_5)]^{2+}$ (oxy-**13**-$O_2CC_6H_5$) [26] and $[Fe_2(\mu\text{-}O_2)\{HB(3,5\text{-}^iPr_2pz)_3\}_2(O_2CCH_2C_6H_5)_2]$ (**17**) [28], have been reported (Fig. 8). The peroxo complex **17** was obtained by a self-assembly of the monomeric iron(II) precursor $[Fe\{HB(3,5\text{-}^iPr_2pz)_3\}(O_2CCH_2C_6H_5)]$ (**18**) in the presence of O_2. In all three complexes, the peroxo ligand bridges two irons in a *cis*-1,2 bridging mode. The iron centers in **16** are doubly bridged by a *cis*-1,2-μ-peroxo group and the μ-alkoxo oxygen of *N*-Et-hptb, whereas those in oxy-**13**-O_2CC_6H have a triply bridged structure with a *cis*-1,2-μ-peroxo group, the μ-phenoxo oxygen, and a μ-benzoato group. The structure of oxy-**13**-O_2CC_6H is similar to that of the μ-peroxo dicobalt complex, $[Co_2(\mu\text{-}O_2)(bpmp)(O_2CC_6H_5)]^{2+}$ (oxy-**1**-$O_2CC_6H_5$) [15].

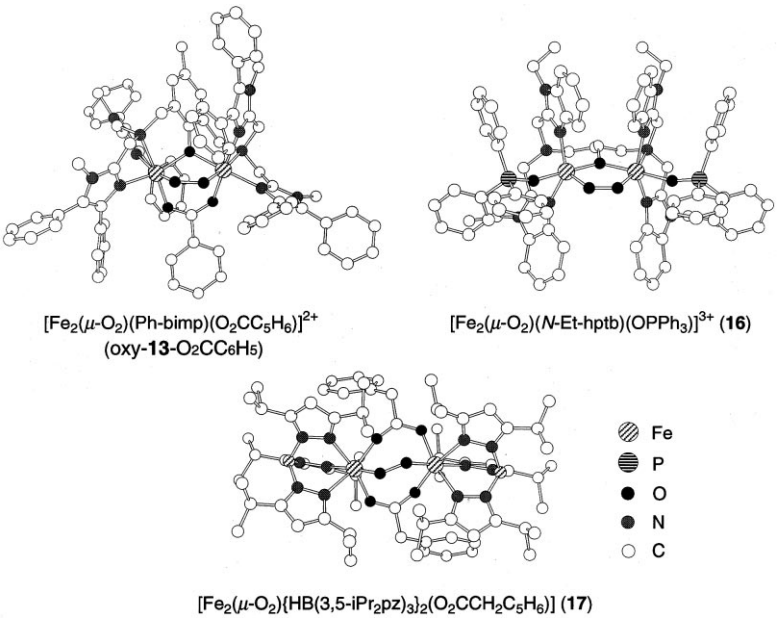

Fig. 8. Structures of μ-peroxo diiron(III) complexes, $[Fe_2(\mu\text{-}O_2)(N\text{-Et-hptb})(OPPh_3)_2]^{3+}$ (**16**), $[Fe_2(\mu\text{-}O_2)(Ph\text{-bimp})(O_2CC_6H_5)]^{2+}$ (oxy-**13**-$O_2CC_6H_5$), and $[Fe_2(\mu\text{-}O_2)\{HB(3,5\text{-}^iPr_2pz)_3\}_2(O_2CCH_2C_6H_5)_2]$ (**17**).

The O–O bond distances of the μ-peroxo diiron complexes described above fall in the range of 1.42 ± 0.01 Å (Table 3), in agreement with the peroxo formulation. For these peroxo complexes each iron center has a distorted octahedral environment with the N_3O_3 donor set. In the case of **16** and **17**, the two metal centers are essentially equivalent with the Fe–O(peroxo) bond distances ranging from 1.880 to

Table 3
Structural features of μ-peroxo diiron(III) complexes

Complex	O–O (Å)	Fe–O_{peroxo} (Å)	Fe···Fe (Å)	Av. Fe–N_{arom} (Å)	Av. Fe–N_{all} (Å)	Refs.
16	1.416(7)	1.880(4)	3.462(3)	2.09	2.18	[27]
oxy-**13**-$O_2CC_6H_5$	1.426(6)	1.864(4), 1.944(4)	3.327(2)	2.16	2.20	[26]
17	1.409(9)	1.876(6), 1.905(6)	4.000(4)	2.18	2.18	[28]
	1.406(9)	1.881(6), 1.877(6)	4.007(4)			
$[Fe_2O(O_2)(L)_2]^{2+}$ [a]			3.14			[37]
oxy-Hr		2.15	3.27		2.20	[9]

[a] L = tris(6-methyl-2-pyridylmethyl)amine.

1.905 Å. In the case of oxy-**13**-$O_2CC_6H_5$ the two iron centers are not equivalent with different Fe–O bond distances (1.944(4) and 1.864(4) Å). The Mössbauer spectrum of oxy-**13**-$O_2CC_6H_5$ exhibits two sets of quadrupole doublets (Table 2), in agreement with the asymmetry of the two iron sites.

The average Fe–N(imidazole) bond distance of oxy-**13**-$O_2CC_6H_5$ (2.16 Å) is substantially longer than that of **16** (2.09 Å). It is also longer than the average of the Fe(III)–N bonds (2.10 Å) and the average of the Fe(II)–N bonds (2.12 Å) in a mixed-valence complex $[Fe_2(bimp)(O_2CC_6H_5)_2]^{2+}$ [48].

The structures of oxy-**13**-$O_2CC_6H_5$, **16**, and **17** indicated that the peroxo ligand is buried within a hydrophobic cavity formed by the phenyl or isopropyl groups, as indicated by a space filling drawing for oxy-**13**-$O_2CC_6H_5$ (Fig. 9). Such a hydrophobic environment about the Fe–O–O–Fe linkage may suppress a thermal decomposition (irreversible oxidation) of the μ-peroxo complex via bimolecular pathways.

3.2.4. Dioxygen affinity of diiron(II) complexes

Thermodynamic studies for the $[M_2(L)(O_2CR)]^{2+}$ type diiron(II) and dicobalt(II) complexes have been reported [19]. The equilibrium constants K for oxygenation were measured by spectrophotometric titration under various dioxygen partial pressures and at different temperatures. Dioxygen affinity of the complexes is dependent upon the nature of the dinucleating ligands and bridging carboxylates. Thermodynamic data are given in Table 4 together with $P(O_2)_{1/2}$ values at 20°C. The $P(O_2)_{1/2}$ values of diiron complexes except for **13**-$O_2CC_6H_5$ are estimated by the extrapolation method using ΔH and ΔS [19]. Although those values, especially for the iron complexes and cobalt complex **7**-O_2CCH_3 which react with dioxygen at low temperature, are only rough measures because of the relatively large standard deviations in enthalpy and entropy, these are convenient for qualitative comparison of dioxygen affinities.

$$[Fe_2] + O_2 \overset{K}{\rightleftharpoons} [Fe_2(\mu\text{-}O_2)] \quad (1)$$

The dioxygen affinity of **12**-$O_2CC_6H_5$, **12**-$O_2CC_6F_5$, and **12**-O_2CCF_3 (having Ph-tidp) varies with the bridging carboxylates: the order is $O_2CC_6H_5 > O_2CC_6F_5 >$

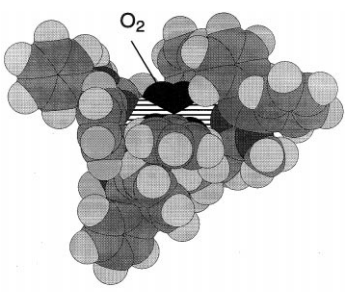

Fig. 9. Space filling view of $[Fe_2(\mu\text{-}O_2)(Ph\text{-}bimp)(O_2CC_6H_5)]^{2+}$ (oxy-**13**-$O_2CC_6H_5$).

Table 4
Thermodynamic data for oxygenation of diiron(II) and dicobalt(II) complexes

Complex	$P(O_2)_{1/2}$ (Torr) at 20°C[a]	ΔH (kJ mol^{-1})	ΔS (J mol^{-1} K^{-1})	Refs.
Diiron complexes				
12-$O_2CC_6H_5$[b]	8600	-55 ± 3	-263 ± 14	[19]
12-$O_2CC_6F_5$[b]	32 000	-55 ± 3	-274 ± 12	[19]
12-O_2CCF_3[b]	77 000	-52 ± 2	-271 ± 6	[19]
11-$C_6H_5CO_2$[b]	ca. 2[d]			[19]
11-O_2CCF_3[b]	5800	-47 ± 3	-231 ± 12	[19]
13-$O_2CC_6H_5$[c]	ca. 2			[26]
Dicobalt complexes				
7-O_2CCH_3[b]	203 000	-76 ± 4	-361 ± 18	[19]
1-$O_2CC_6F_5$[c]	2.6	-93 ± 3	-324 ± 11	[19]
1-O_2CCF_3[c]	27	-65 ± 3	-251 ± 10	[19]
Hr (*Phascolopsis*)	ca. 2.2	-52	-75	[49]
Hc (*Helix pomatia* R)	ca. 2.7	-48	-53	[49]

[a] $P(O_2)_{1/2}$ represents the dioxygen partial pressure (Torr) at which half amount of complex is oxygenated (standard state is 1 Torr at 20°C). The values given for iron complexes except for **13**-$O_2CC_6H_5$ and that for cobalt complex **7**-O_2CCH_3 are estimated by the extrapolation method using ΔH and ΔS [19].
[b] In dichloromethane.
[c] In acetonitrile.
[d] At -40°C.

O_2CCF_3. This order can be explained by the electron-donating ability of the bridging carboxylates and is in agreement with the general observation that dioxygen affinity is enhanced by a stronger electron donor [13,14].

The dioxygen affinity for **11**-O_2CCF_3 (with Me_4-tpdp) and **13**-$O_2CC_6H_5$ (with Ph-bimp) is larger than that for the Ph-tidp complexes (**12**-$O_2CC_6H_5$, **12**-$O_2CC_6F_5$, and **12**-O_2CCF_3), though the Me_4-tpdp and Ph-bimp ligands are weak electron-donors compared with the Ph-tidp ligand. This is in contrast to the trend in the dioxygen affinity observed for the Ph-tidp complexes with different bridging carboxylates. The enthalpy change for the oxygenation of **11**-O_2CCF_3 (-47 kJ mol^{-1}) is more positive (less favorable) than those for the Ph-tidp complexes (-52 to -55 kJ mol^{-1}), whereas the entropy change for the oxygenation of **11**-O_2CCF_3 (-231 J mol^{-1} K^{-1}) is less negative (more favorable) than those for the Ph-tidp complexes (-263 to -274 J mol^{-1} K^{-1}). The favorable entropy change for the oxygenation of **11**-O_2CCF_3 overcomes the unfavorable enthalpy change, leading to high dioxygen affinity for this complex relative to the Ph-tidp complexes.

The dioxygen affinity of **13**-$O_2CC_6H_5$ is exceptionally high compared to those of the Me_4-tpdp and Ph-tidp complexes, which is more than 3×10^3–4×10^4 times greater than that of the Me_4-tpdp and Ph-tidp complexes at 20°C [19,26]. However, thermodynamic parameters have not been obtained for **13**-$O_2CC_6H_5$.

3.2.5. Comparison in dioxygen affinity between diiron and dicobalt complexes

Reactivity of iron complexes toward dioxygen is much higher than that of corresponding cobalt complexes with the same ligand system. For example, the diiron(II) complex **11**-$O_2CC_6H_5$ forms oxy-**11**-$O_2CC_6H_5$ at -40°C, whereas the corresponding dicobalt(II) complex $[Co_2(Me_4\text{-tpdp})(O_2CCH_3)]^{2+}$ (**19**) has no reactivity toward O_2. It is suggested that the electron density on the cobalt(II) in **19** is not high enough to produce O_2^{2-} [19]. Thus, strong electron donors are necessary for oxygenation of cobalt(II) complexes. In contrast to **19**, $[Co_2(tpdp)(O_2CCH_3)]^{2+}$ (**7**-O_2CCH_3) is shown to react with O_2 below 0°C in CH_2Cl_2 to form oxy-**7**-O_2CCH_3.

However, the dioxygen affinity of **7**-O_2CCH_3 is extremely low compared with the diiron complexes of Me_4-tpdp and Ph-tidp. The enthalpy change associated with the oxygenation of **7**-O_2CCH_3 is -76 kJ mol^{-1} which is significantly more negative (favorable) than those for the diiron complexes (-47 to -55 kJ mol^{-1}), whereas the loss in entropy for the oxygenation of **7**-O_2CCH_3 (-361 J mol^{-1} K^{-1}) is significantly larger than those for the diiron complexes (-231 to -274 J mol^{-1} K^{-1}) (see Table 4). The unfavorable entropy change in the oxygenation of **7**-O_2CCH_3 can not be compensated with the enthalpic stabilization, resulting in a low dioxygen affinity of this complex. The observed enthalpic stabilization for **7**-O_2CCH_3 can partly be ascribed to the ligand field stabilization effect. In the case of cobalt complexes, the oxygenation of a dicobalt(II) complex accompanies the change from high-spin Co(II) to low-spin Co(III) to provide a large ligand field stabilization. In the case of iron complexes, no spin-change at the metal center occurs upon oxygenation and high-spin Fe(III) has no ligand field stabilization. Such an enthalpic stabilization is also found for the oxygenation of the bpmp dicobalt complexes (**1**-O_2CCF_3, **1**-$O_2CC_6F_5$). The bonding contribution in ΔH associated with oxygenation of **7**-O_2CCH_3 may restrict molecular freedom, leading to a decrease in entropy. Thus, the low dioxygen affinity of **7**-O_2CCH_3 compared with the Me_4-tpdp and Ph-tidp diiron complexes is partly attributable to an unfavorable entropy effect.

The dioxygen affinity of $[Co_2(bpmp)(O_2CCF_3)]^{2+}$ (**1**-O_2CCF_3) (the ligand has the 2,6-bis(aminomethyl)phenolate bridging skeleton) is extremely high compared with that of **7**-O_2CCH_3 (1,3-diamino-2-propanolate bridging skeleton). The enthalpy change for the oxygenation of **1**-O_2CCF_3 (-65 kJ mol^{-1}) is smaller than that for the oxygenation of **7**-O_2CCH_3 (-76 kJ mol^{-1}), whereas the entropy change for the oxygenation of **1**-O_2CCF_3 (-251 J mol^{-1} K^{-1}) is significantly less negative (favorable) than that for the oxygenation of **7**-O_2CCH_3 (-361 J mol^{-1} K^{-1}). Thus, the entropic stabilization derives a high dioxygen affinity for **1**-O_2CCF_3.

The above thermodynamic results for **1**-O_2CCF_3 and **7**-O_2CCH_3 suggest that the geometric feature of bridging skeleton is important for controlling dioxygen affinity. The structures of the μ-1,2-peroxo dicobalt and diiron complexes with 'end-off' compartmental ligands reveals that the metal···metal separation is constrained to ca. 3.1–3.46 Å [15,18,26,27]. The metal···metal separations of the diiron(II) complexes with bpmp and Ph-bimp analogs (the 2,6-bis-(aminomethyl)phenolate bridging skeleton) are generally less than 3.4 Å ([Fe_2(5-

Me-HXTA)(μ-OH)(H_2O)$_2$], 3.137 Å [50], [Fe_2(bpmp)($O_2CC_2H_5$)$_2$]$^+$, 3.365 Å [51]). The ligands containing the 1,3-diamino-2-propanolate bridging skeleton tend to expand the metal···metal distance (>3.45 Å); the metal···metal distances for **10**-$O_2CC_6H_5$, **11**-$O_2CC_6H_5$, and **12**-$O_2CC_6H_5$ are 3.47, 3.68, and 3.59 Å, respectively, [19,24,25,52]. Oxygenation for **10**-$O_2CC_6H_5$, **11**-$O_2CC_6H_5$, and **12**-$O_2CC_6H_5$ necessitates a substantial stereochemical change, and this may be responsible for the observed low dioxygen affinity of the complexes.

4. Dicopper dioxygen complexes

Various types of dioxygen (peroxo and superoxo) copper(II) complexes have been reported [53–58]. In this section, dicopper(II)–dioxygen complexes derived from 'end-off' compartmental ligands are described.

It is found by Karlin et al. that phenol-based compartmental ligands of 'end-off' type can be formed when dicopper(I) complexes of non-compartmental ligands (R–XYL–H), having two metal-binding sites separated by an aromatic spacer, are oxygenated (Fig. 10). Reaction of [Cu_2(R–XYL–H)]$^{2+}$ (**20**) with O_2 produces [Cu_2(R–XYL–O)(OH)]$^{2+}$ (**21**) in a high yield ($>95\%$ for H–XYL–H) [59–61]. Various physicochemical investigations for the oxygenation of **20**, including low-temperature stopped-flow kinetics and resonance Raman spectroscopy, have revealed that the copper(I) complexes reversibly bind O_2 at low temperatures (below -80°C) to generate a μ-η^2:η^2-peroxo (side on) intermediate having a bent 'butterfly' core structure. The intermediate exhibits characteristic absorption bands attributable to peroxo(π^*_σ)-to-Cu(II) LMCT transitions at ca. 360 and ca. 440 nm,

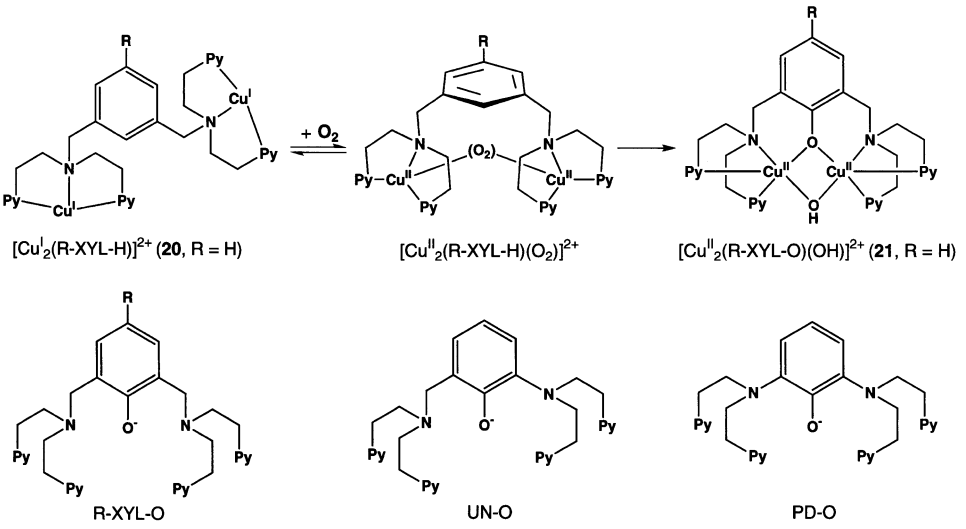

Fig. 10. Oxygenation and hydroxylation of [Cu_2(R–XYL–H)]$^{2+}$ (**20**) with O_2 and 'end-off' compartmental ligands derived from hydroxylation by dicopper(I)/O_2 system.

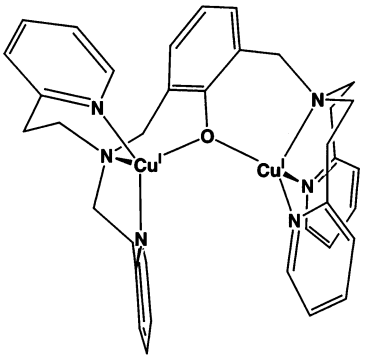

Fig. 11. Structure of $[Cu_2(H–XYL–O)]^+$ (**22**).

and a ν(O–O) Raman band is observed at 747 cm^{-1} for NO_2–XYL–H [61–63]. The peroxo group of the intermediate hydroxylates the adjacent xylyl group to form the phenol-based compartmental ligands, R–XYL–O [63]. Similarly, the asymmetric UN–O and symmetric PD–O 'end-off' compartmental ligands have been synthesized by the hydroxylation of the xylyl group with the 'activated' peroxo group [64,65]. Analogous 'end-off' compartmental ligands containing pyrazole or mixed pyrazole/pyridine groups as the side arms were obtained by Sorrell et al. [66].

Dioxygen binding for a dicopper(I) complex of H–XYL–O, $[Cu_2(H–XYL–O)]^+$ (**22**), has been investigated by Karlin et al. [67]. In the crystal structure of **22** there exist two crystallographically independent molecules of similar structures whose Cu···Cu separations linked by a phenoxo bridge are 3.619 and 3.715 Å (Fig. 11). Each copper(I) has a four-coordinate trigonal-pyramidal structure with a bridging phenoxo oxygen in the basal plane. The complex has a reaction site on each copper(I) ion with O_2. Complex **22** binds O_2 (Cu:O_2 = 2:1) in CH_2Cl_2 at -80°C to produce a deep-purple species $[Cu_2(O_2)(H–XYL–O)]^+$ (**23**) (λ_{max}/nm (ε/M^{-1} cm^{-1}); 385 (2900), 505 (6000), 610 (shoulder, 2100), 790 (700), 925 (600)). The presence of a peroxo ligand in **23** is indicated by resonance Raman spectroscopy (ν(O–O) = 803 cm^{-1}) [68]. The Cu···Cu separation of 3.31 Å determined by EXAFS studies [69] and resonance Raman studies using ^{16}O–^{18}O [68] suggest that the peroxo ligand coordinates to one copper ion or bridges the metal ions in an asymmetric mode as shown in Scheme 2. Resonance Raman excitation profile studies indicate that two intense absorption bands at 505 and 610 nm are attributable to the peroxo(π^*_σ)-to-Cu(II) and peroxo(π^*_ν)-to-Cu(II) LMCT transitions, respectively [68]. Oxygenation–deoxygenation for **22** is almost reversible. It is oxygenated in CH_2Cl_2 at -80°C and then deoxygenated by evacuating the oxygenated solution while warming to room temperature [67]. Complex **23** reacts with CO to produce a dicarbonyl dicopper(I) complex, $[Cu_2(H–XYL–O)(CO)_2]^+$ (**24**), which is decarbonylated in vacuo to give **22**. Thus, the **23** → **24** → **22** → **23** cycle is established, and this cycle is repeated many times. Reaction of **23** with PPh_3

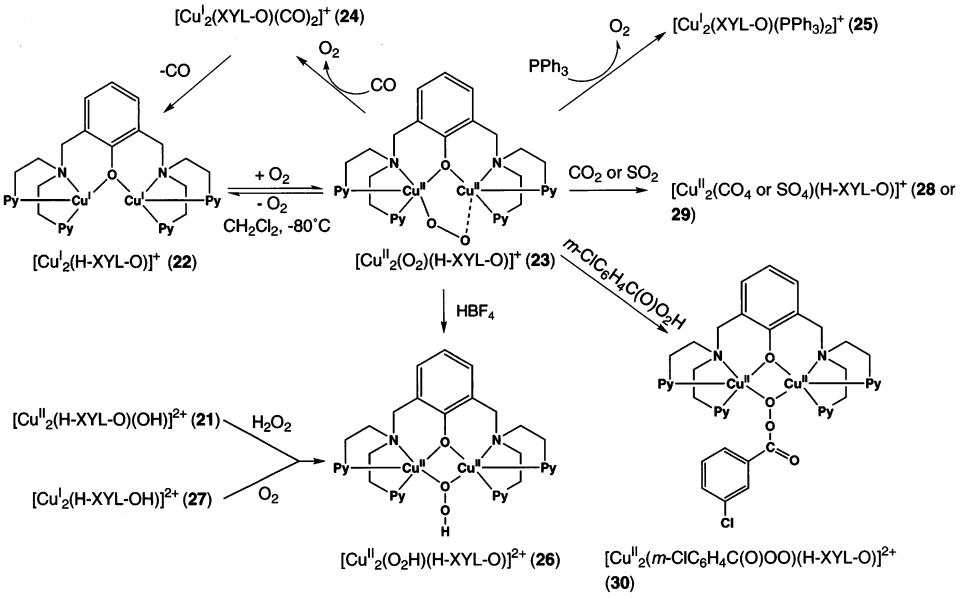

Scheme 2. Reversible oxygenation of $[Cu_2(H–XYL–O)]^+$ (**22**) and reactivity of $[Cu_2(O_2)(H–XYL–O)]^+$ (**23**).

liberates O_2 to form a dicopper(I) complex $[Cu_2(H–XYL–O)(PPh_3)_2]^+$ (**25**). This means that the peroxo group in **23** can not oxidize PPh_3. Upon decomposition of **23**, $[Cu_2(H–XYL–O)(OH)]^{2+}$ (**21**) is obtained.

Kinetic studies for the O_2 binding of **22** reveal that the 'on-rate' is too fast to be measured ($k_{on} > 10^6$ M^{-1} s^{-1}) even at -100°C [62]; it is 10^4 times faster than the on-rate of $[Cu_2(R–XYL–H)]^{2+}$ (**20**) where the two copper(I) ions are not fixed in close proximity. It is evident that the 'end-off' compartmental ligand binds two copper(I) centers in close proximity, providing a geometrical preference for the dicopper(I) core to bind dioxygen.

The peroxo ligand in **23** is basic (nucleophilic) and reacts with HBF_4 to produce a hydroperoxo dicopper(II) complex $[Cu_2(O_2H)(H–XYL–O^-)]^{2+}$ (**26**) (Scheme 2) [70,71]. This hydroperoxo complex **26** can also be obtained by either the oxygenation of the dicopper(I) complex $[Cu_2(H–XYL–OH)]^{2+}$ (**27**) (the phenolic group being free from bridging) or the substitution of the μ-hydroxo ligand in the μ-hydroxo dicopper(II) complex **21** for the peroxo group. The Cu···Cu separation of **26** (3.04 Å from EXAFS) suggests the hydroperoxo ligand to assume a μ-1,1-bridging mode like the bridging OH^- in **21** (Cu···Cu = 3.082 Å) [60]. The electronic spectrum of **26** differs from that of **23** and exhibits absorption bands at 395 ($\varepsilon = 8000$), 450 (shoulder, $\varepsilon = 2200$), 620 ($\varepsilon = 450$), and 860 nm (shoulder, $\varepsilon = 50$ M^{-1} cm^{-1}).

The complex (**26**) is stable in CH_2Cl_2 at -80°C for several days, but decomposed to $[Cu_2(H–XYL–O)(Cl)]^{2+}$ upon warming. This fact means that the complex reacts

with CH_2Cl_2 upon thermal decomposition. On the other hand, in acetonitrile or propionitrile solvents the thermal decomposition of **26** afforded the hydroxo-bridged complex **21** in high yield. This suggests the disproportionation of the hydroperoxo complex, $2[Cu_2(O_2H)(H\text{–}XYL\text{–}O)]^{2+}$ (**26**) $\rightarrow 2[Cu_2(H\text{–}XYL\text{–}O)(OH)]^{2+} + O_2$. However, dioxygen was not detected in the thermal decomposition of **26** [70b].

Complex **23** reacts with CO_2 and SO_2 to produce a peroxycarbonato complex $[Cu_2(CO_4)(H\text{–}XYL\text{–}O)]^{+}$ (**28**) and a sulfato complex $[Cu_2(SO_4)(H\text{–}XYL\text{–}O)]^{+}$ (**29**), respectively [70b,71]. Furthermore, **23** reacts with RC(O)Cl in CH_2Cl_2 at -80°C to generate acylperoxo dicopper(II) complexes $[Cu_2(OO(O)CR)(H\text{–}XYL\text{–}O)]^{2+}$ [72]. The crystal structure of $[Cu_2(m\text{-}ClC_6H_4C(O)OO)(H\text{–}XYL\text{–}O)](ClO_4)_2 \cdot CH_3CN$ (**30**) has been determined. The two copper(II) ions are linked by the phenoxo and m-$ClC_6H_4C(O)OO$ groups, where the acylperoxo ligand assumes a μ-1,1-bridging mode as proposed for the μ-O_2H in $[Cu_2(O_2H)(R\text{–}XYL\text{–}O)]^{2+}$ (**26**) [70]. The Cu···Cu separation in **30** is 3.197 Å, which is longer than that in **26** (3.04 Å). The O–O bond distance in the m-$ClC_6H_4C(O)OO$ group is 1.46 Å, which is normal for peroxo O–O bonds.

Both the hydroperoxo and acylperoxo complexes, **26** and **30**, can oxidize PPh_3 and RSR (RSR = tetrahydrothiophene), whereas the peroxo complex (**23**) cannot oxidize PPh_3 [70–72]. It is suggested that hydroperoxo and acylperoxo complexes or some derivatives derived from the O–O bond cleavage can be intermediates in metal-catalyzed oxidation using dioxygen, hydrogen peroxide, or acylperoxide.

Karlin et al. reported a reversible oxygenation for $[Cu_2(UN\text{–}O)]^{+}$ (**31**) derived from an asymmetric 'end-off' compartmental ligand UN–O [73]. The structure of **31** is similar to that of **22**, but the Cu···Cu separation (3.569 Å) of the former is slightly shorter than those of the latter (3.619 and 3.715 Å for two crystallographically independent molecules). Complex **31** reacts with O_2 ($Cu{:}O_2 = 2{:}1$) in CH_2Cl_2 at -80°C to generate intense-purple species $[Cu_2(O_2)(UN\text{–}O)]^{+}$ (**32**). The Cu···Cu separation of **32** determined from EXAFS is 3.28 Å that is compared to that of **23** (3.31 Å). It is suggested that the peroxo ligand in **32** adopts a terminal binding mode or an asymmetric bridging mode as supposed for **23**. The electronic spectrum of **32** resembles that of **23** and exhibits LMCT bands at 392 ($\varepsilon = 3400$), 510 ($\varepsilon = 5400$), and 642 nm ($\varepsilon = 2700\ M^{-1}\ cm^{-1}$). Notably, **32** is thermally very stable against irreversible oxidation. Thus, the stereochemistry of the dinucleating ligand also has a significant influence on the thermal stability of the peroxo species as found for the other previously described peroxo metal complexes.

Complex **32** is converted into a superoxo dicopper(II) complex $[Cu^{II}_2(O_2)(UN\text{–}O)]^{2+}$ (**33**) (λ_{max}; 404 nm ($\varepsilon = 5400\ M^{-1}\ cm^{-1}$)) when oxidized with Ag^{+}. On the other hand, a mixed-valence complex $[Cu^{I}Cu^{II}(UN\text{–}O)]^{2+}$ (**34**) is derived from **31** by one-electron oxidation with ferrocenium ion (Scheme 3) [74]. Reversible oxygenation–deoxygenation between **33** and **34** is reported at -80°C.

The peroxo ligand in **32** is basic enough to react with HBF_4 to give a hydroperoxo complex $[Cu_2(O_2H)(UN\text{–}O)]^{2+}$ (**35**), which shows absorption bands at 395 ($\varepsilon = 7000\ M^{-1}\ cm^{-1}$) and 650 nm ($\varepsilon = 660\ M^{-1}\ cm^{-1}$). EXAFS studies for this complex indicate a Cu···Cu separation of 2.95 Å [73]. A μ-1,1-bridging mode of the

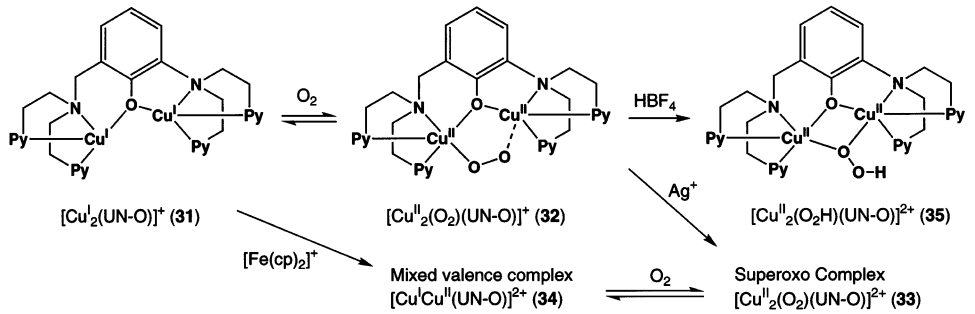

Scheme 3. Oxygenation and chemical conversions of $[Cu_2(UN–O)]^+$ (**31**).

hydroperoxo group is considered for **35** based on the marked resemblance between **35** and **26** in the spectral and EXAFS data. The absorption band at 395 nm ($\varepsilon = 7000\ M^{-1}\ cm^{-1}$) is assigned to the hydroperoxo(π*)-to-Cu(II) LMCT transition [75]. This LMCT transition is ca. 5000 cm^{-1} higher in energy than that of the unprotonated complex **32** (510 nm). This is due to the stabilization of the antibonding peroxo π* orbitals by the protonation. The resonance Raman spectrum for **35** reveals an O–O stretching vibration at 892 cm^{-1}, which is higher than the ν(O–O) vibrations observed for peroxo dicopper complexes. For example, the ν(O–O) vibration of **23** is seen at 803 cm^{-1}. It is explained by Solomon et al. that the protonation reduces the electron-density on the antibonding peroxo π* orbitals and leads to an increase in the O–O bond order.

Karlin et al. classified peroxo dicopper complexes into two categories depending on their reactivity; basic/nucleophilic peroxides and non-basic/electrophilic peroxides (Scheme 4) [71]. Peroxo groups in a terminal-binding or an asymmetric-bridging mode as proposed for **23** and **32** and those in a *trans*-μ-1,2-bridging mode as found for $[Cu_2(\mu\text{-}O_2)(tpa)_2]^{2+}$ [76] are basic/nucleophilic; they react with electrophiles but can not oxidize nucleophilic substrates such as PPh_3. Peroxo groups in a $\mu\text{-}\eta^2\text{:}\eta^2$-bridging mode are non-basic/electrophilic; they hardly react with electrophiles but can oxidize nucleophilic substrates such as PPh_3 and the xylyl group in $[Cu_2(R–XYL–H)]^{2+}$ (**20**). As mentioned above, the hydroperoxo complexes, **26** and **35**, oxidize PPh_3 and RSR (tetrahydrothiophene) [70–73], whereas the deprotonated peroxo complexes, **23** and **32**, cannot oxidize these substrates. Thus, the hydroperoxo groups in **26** and **35** are electrophilic in nature. Based on electronic structural considerations, Solomon et al. have rationalized the nature of the μ-1,1-hydroperoxo group as electrophilic [75].

Rare μ_4-peroxo tetracopper(II) complexes $[Cu_4(\mu\text{-}O_2)(L^n)_2(OMe)_2(ClO_4)]^+$ (**36**) have been synthesized by Krebs et al. (Fig. 12) [77], by the reaction of a ligand L^n and copper(II) perchlorate in methanol in the presence of hydrogen peroxide or 3,5-di-*tert*-butylcatechol. In the latter case, peroxide is generated by the reduction of O_2 with 3,5-di-*tert*-butylcatechol, catalyzed by a copper(II) ion. The peroxo ligand assumes a $\mu_4\text{-}(\eta^1)_4$-bridging mode to four copper(II) ions, forming a novel roofed Cu_4O_4 core. The O–O bond distance is 1.453 Å, which is characteristic of the

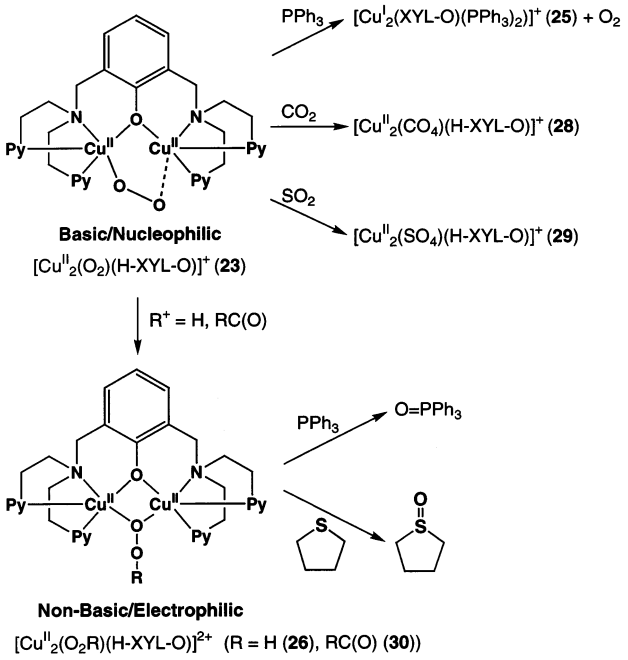

Scheme 4. Difference in chemical reactivity between $[Cu_2(O_2)(H–XYL–O)]^+$ (**23**) and $[Cu_2(O_2R)$-$(H–XYL–O)]^{2+}$ (R = H (**26**), RC(O) (**30**)).

peroxo complexes. The complexes exhibit a O–O stretching vibration at 878–898 cm^{-1}, which is compared well with the O–O vibration of **35** (892 cm^{-1}) [75]. However, the O–O vibration of **36** is substantially higher than those for the μ-η^2:η^2-peroxo complexes (730–760 cm^{-1}) [56], *trans*-μ-1,2-peroxo complex, $[Cu_2(\mu\text{-}O_2)(tpa)_2]^{2+}$, (832 cm^{-1}) [78], and **23** (803 cm^{-1}) [68]. Such μ_4-peroxo complexes can be a model for the water oxidation in photosystem II and also for a bimolecular thermal decomposition of the μ-peroxo diiron(III) complexes as described Section 3.2.2 [44].

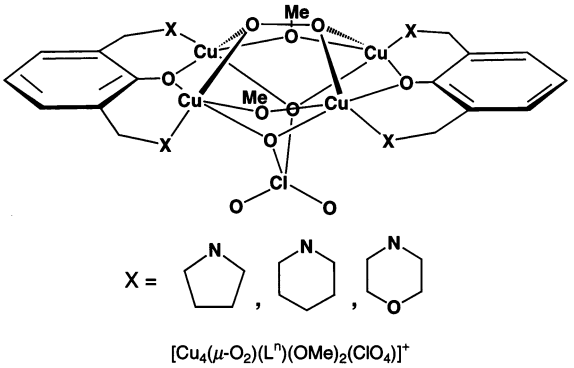

Fig. 12. Structure of $[Cu_4(\mu\text{-}O_2)(L^n)_2(OMe)_2(ClO_4)]^+$ (**36**).

5. Summary

The chemistry of bimetallic dioxygen complexes is of particular importance for understanding the role of the active bimetallic centers of dioxygen binding and activating metalloproteins in biological systems and in utilizing metal complexes as oxidation catalyst. 'End-off' compartmental ligands have been shown to be useful in controlling dioxygen binding chemistry by bimetallic complexes. Control of the thermal stability of the dioxygen complexes against irreversible oxidation, reversible binding of dioxygen, and dioxygen affinity by bimetallic complexes has been achieved to some extent by electronic and stereochemical modification of the 'end-off' compartmental ligands. For a more complete understanding of this chemistry, however, further systematic and detailed investigation of the formation and decomposition processes of various types of dioxygen complexes are needed. Such studies may provide valuable guidelines into the molecular modeling of ligand environments for control of these processes and may also give new insight into dioxygen activation by bimetallic complexes.

Acknowledgements

This work was supported by a Grant-in-Aid for Scientific Research on Priority Area 'Metal-assembled Complexes' (M.S. and H.Ō.) and by a JSPS Research Fellowship for Young Scientists (H.F) from the Ministry of Education, Science, and Culture, Japan.

References

[1] U. Casellato, P.A. Vigato, M. Vidali, Coord. Chem. Rev. 23 (1977) 31.
[2] P. Zanello, S. Tanburini, P.L. Vigato, G.A. Mazzocchin, Coord. Chem. Rev. 77 (1987) 165.
[3] P.A. Vigato, S. Tamburini, D.E. Fenton, Coord. Chem. Rev. 106 (1990) 25.
[4] D.E. Fenton, H. Ōkawa, Perspect. Bioinorg. Chem. 2 (1993) 81.
[5] D.E. Fenton, H. Ōkawa, Chem. Ber. Recl. 130 (1997) 433.
[6] H. Ōkawa, H. Furutachi, D.E. Fenton, Coord. Chem. Rev. 174 (1998) 51.
[7] S.R. Collinson, D.E. Fenton, Coord. Chem. Rev. 148 (1996) 19.
[8] K.A. Magnus, H. Ton-That, J.E. Carpenter, Chem. Rev. 94 (1994) 725.
[9] R.E. Stenkamp, Chem. Rev. 94 (1994) 715.
[10] E.I. Solomon, M.M. Sundaram, T.E. Machonkin, Chem. Rev. 96 (1996) 2563.
[11] B.J. Wallar, J.D. Lipscomb, Chem. Rev. 96 (1996) 2625.
[12] G. McLendon, A.E. Martell, Coord. Chem. Rev. 19 (1976) 1.
[13] R.D. Jones, D.A. Summerville, F. Basolo, Chem. Rev. 79 (1979) 139.
[14] E.C. Niederhoffer, J.H. Timmons, A.E. Martell, Chem. Rev. 84 (1984) 137.
[15] M. Suzuki, I. Ueda, H. Kanatomi, I. Murase, Chem. Lett. (1983) 185.
[16] M. Suzuki, H. Kanatomi, I. Murase, Bull. Chem. Soc. Jpn. 57 (1984) 36.
[17] M. Suzuki, T. Sugisawa, A. Uehara, Bull. Chem. Soc. Jpn. 63 (1990) 1115.
[18] K. Kayatani, Y. Hayashi, M. Suzuki, A. Uehara, Bull. Chem. Soc. Jpn. 67 (1994) 2980.
[19] H. Sugimoto, T. Nagayama, S. Maruyama, S. Fujinami, Y. Yasuda, M. Suzuki, A. Uehara, Bull. Chem. Soc. Jpn. 71 (1998) 2267.

[20] M. Suzuki, unpublished data.
[21] M. Suzuki, S. Fujinami, T. Hibino, H. Hori, Y. Maeda, A. Uehara, M. Suzuki, Inorg. Chim. Acta 238 (1998) 124.
[22] L. Que Jr., J. Chem. Soc. Dalton Trans. (1997) 3933.
[23] (a) N. Kitajima, H. Fukui, Y. Moro-oka, Y. Mizutani, T. Kitagawa, J. Am. Chem. Soc. 112 (1990) 6402. (b) N. Kitajima, N. Tamura, H. Amagai, H. Fukui, Y. Moro-oka, Y. Mizutani, T. Kitagawa, R. Mathur, K. Heerwegh, C.A. Reed, C.R. Randall, L. Que Jr., K. Tatsumi. J. Am. Chem. Soc. 116 (1994) 9071.
[24] (a) S. Ménage, B.A. Brennan, C. Juarez-Garcia, E. Münck, L. Que Jr., J. Am. Chem. Soc. 112, (1990) 6423. (b) Y. Dong, S. Ménage, B.A. Brennan, T.E. Elgren, H.G. Jang, L.L. Pearce, L. Que Jr., J. Am. Chem. Soc. 115 (1993) 1851.
[25] (a) Y. Hayashi, M. Suzuki, A. Uehara, Y. Mizutani, T. Kitagawa, Chem. Lett. (1992) 91. (b) Y. Hayashi, T. Kayatani, H. Sugimoto, M. Suzuki, K. Inomata, A. Uehara, Y. Mizutani, T. Kitagawa, Y. Maeda, J. Am. Chem. Soc. 117 (1995) 11220.
[26] T. Ookubo, H. Sugimoto, T. Nagayama, H. Masuda, T. Sato, K. Tanaka, Y. Maeda, H. Ōkawa, Y. Hayashi, A. Uehara, M. Suzuki, J. Am. Chem. Soc. 118 (1996) 701.
[27] Y. Dong, S. Yan, V.G. Young Jr., L. Que Jr., Angew. Chem. Int. Ed. Engl. 35 (1996) 618.
[28] K. Kim, S.J. Lippard, J. Am. Chem. Soc. 118 (1996) 4914.
[29] Y. Nishida, M. Takeuchi, S. Kida, Inorg. Chim. Acta 96 (1984) 115.
[30] Y. Nishida, M. Takeuchi, Z. Naturforsch. Teil B 42 (1987) 52.
[31] B.A. Brennan, Q. Chen, C. Juarez-Garcia, A.E. True, C.J. O'Connor, L. Que Jr., Inorg. Chem. 30 (1991) 1937.
[32] B.P. Murch, F.C. Bradley, L. Que Jr., J. Am. Chem. Soc. 108 (1986) 5027.
[33] M. Suzuki et al., to be submitted.
[34] M. Suzuki, A. Uehara, H. Oshio, K. Endo, M. Yanaga, S. Kida, K. Saito, Bull. Chem. Soc. Jpn. 60 (1987) 3547.
[35] M. Suzuki, H. Oshio, A. Uehara, K. Endo, M. Yanaga, S. Kida, K. Saito, Bull. Chem. Soc. Jpn. 61 (1988) 3907.
[36] M. Suzuki et al., to be submitted.
[37] Y. Dong, Y. Zang, L. Shu, E.C. Wilkinson, L. Que Jr., K. Kauffmann, E. Münck, J. Am. Chem. Soc. 119 (1997) 12683.
[38] J. Sanders-Loehr, in: T.M. Loehr Jr. (Ed.), Iron Carriers and Iron Proteins, VCH, New York, 1989, pp. 375–466.
[39] K.E. Liu, D. Wang, B.H. Huynh, D.E. Edmondson, A. Salifoglou, S.J. Lippard, J. Am. Chem. Soc. 116 (1994) 7465.
[40] K.E Liu, A.M Valentine, D. Qiu, D.E. Edmondson, E.H Appelman, T.G. Spiro, S.J. Lippard, J. Am. Chem. Soc. 117 (1995) 4997.
[41] J.M. Bollinger Jr., C. Krebs, A. Vicol, S. Chen, B.A. Ley, D.E. Edmondson, B.H. Huynh, J. Am. Chem. Soc. 120 (1998) 1094.
[42] P. Moënne-Loccoz, J. Baldwin, B.A. Ley, T.M. Loehr, J.M. Bollinger Jr., Biochemistry 37 (1998) 14659.
[43] J.A. Broadwater, J. Ai, T.M. Loehr, J. Sanders-Loehr, B.G. Fox, Biochemistry 37 (1998) 14664.
[44] A.L. Feig, M. Becker, S. Schindler, R. van Eldik, S.J. Lippard, Inorg. Chem. 35 (1996) 2590.
[45] A.L. Feig, M. Becker, A. Masschelein, A. Bakac, S.J. Lippard, J. Am. Chem. Soc. 119 (1997) 334.
[46] J.R. Hagadorn, L. Que, W.B. Tolman, I. Prisecaru, E. Münck, J. Am. Chem. Soc. 121 (1999) 9760.
[47] D. Lee, J.D. Bois, D. Petasis, M.P. Hendrich, C. Krebs, B.H. Huynh, S.J. Lippard, J. Am. Chem. Soc. 121 (1999) 9893.
[48] M.S. Mashuta, R.J. Webb, J.K. McCusker, E.A. Schmitt, K.J. Oberhausen, J.F. Richardson, R.M. Buchanan, D.N. Hendrickson, J. Am. Chem. Soc. 114 (1992) 3815.
[49] G.B. Jameson, J.A. Ibers, in: I. Bertini, H.B. Gray, S.J. Lippard, J.S. Valentine Jr. (Eds.), Bioinorganic Chemistry, University Science Books, Sausalito, 1994, pp. 167–252.
[50] B.P. Murch, F.C. Bradley, P.D. Boyle, V. Papaefthymiou, L. Que Jr., J. Am. Chem. Soc. 109 (1987) 7993.
[51] A.S. Borovik, V. Papaefthymiou, L.F. Taylor, O.P. Anderson, L. Que Jr., J. Am. Chem. Soc. 111 (1989) 6183.

[52] (a) D.L. Jameson, C.L. Xie, D.N. Hendrickson, J.A. Potenza, H.J. Schugar, J. Am. Chem. Soc. 109 (1987) 740. (b) Q. Chen, J.B. Lynch, P.G. Romero, A.B. Hussein, G.B. Jameson, C.J. O'Conner, L. Que Jr., Inorg. Chem. 27 (1988) 2673. (c) M. Suzuki, T. Sugisawa, H. Senda, H. Oshio, A. Uehara, Chem. Lett. 1091 (1989). (d) M. Suzuki, H. Senda, M. Suenaga, T. Sugisawa, A. Uehara, Chem. Lett. (1990) 923. (e) S. Kawata, M. Nakamura, Y. Yamashita, K. Asai, K. Kikuchi, I. Ikemoto, M. Katata, H. Sano, Chem. Lett. (1992) 135.
[53] K.D. Karlin, A.D. Zuberbühler, in: J. Reedijk, E. Bouwman (Eds.), Bioinorganic Catalysis, 2nd ed., Marcel Dekker, New York, 1999, pp. 469–534.
[54] K.D. Karlin, S. Kaderli, A.D. Züberbühler, Acc. Chem. Res. 30 (1997) 139.
[55] N. Kitajima, Adv. Inorg. Chem. 39 (1992) 1.
[56] N. Kitajima, Y. Moro-oka, Chem. Rev. 94 (1994) 737.
[57] W.B. Tolman, Acc. Chem. Res. 30 (1997) 227.
[58] M.A. Kopf, K.D. Karlin, in: B. Meunier (Ed.), Biomimetic Oxidations, Imperial College Press, London, 2000, pp. 309–362.
[59] K.D. Karlin, P.L. Dahlstrom, S.N. Cozzette, P.M. Scensny, J. Zubieta, J. Chem. Soc. Chem. Commun. (1981) 881.
[60] K.D. Karlin, J.C. Hayes, Y. Gultneh, R.W. Cruse, J.W. McKown, J.P. Hutchinson, J. Zubieta, J. Am. Chem. Soc. 106 (1984) 2121.
[61] K.D. Karlin, M.S. Nasir, B.I. Cohen, R.W. Cruse, S. Kaderli, A.D. Zuberbühler, J. Am. Chem. Soc. 116 (1994) 1324.
[62] R.W. Cruse, S. Kaderli, K.D. Karlin, A.D. Zuberbühler, J. Am. Chem. Soc. 110 (1988) 6882.
[63] E. Pidcock, H.V. Obias, C.X. Zhang, K.D. Karlin, E.I. Solomon, J. Am. Chem. Soc. 120 (1998) 7841.
[64] M.S. Nasir, K.D. Karlin, D. McGowty, J. Zubieta, J. Am. Chem. Soc. 113 (1991) 698.
[65] N.N. Murthy, M. Mahroof-Tahir, K.D. Karlin, J. Am. Chem. Soc. 115 (1993) 10404.
[66] T.N. Sorrell, V.A. Vankai, Inorg. Chem. 29 (1990) 1687.
[67] K.D. Karlin, R.W. Cruse, Y. Gultneh, A. Farooq, J.C. Hayes, J. Zubieta, J. Am. Chem. Soc. 109 (1987) 2668.
[68] J.E. Pate, R.W. Cruse, K.D. Karlin, E.I. Solomon, J. Am. Chem. Soc. 109 (1987) 2624.
[69] N.J. Blackburn, R.W. Strange, R.W. Cruse, K.D. Karlin, J. Am. Chem. Soc. 109 (1987) 1235.
[70] (a) K.D. Karlin, R.W. Cruse, Y. Gultneh, J. Chem. Soc. Chem. Commun. (1987) 599. (b) K.D. Karlin, P. Ghosh, R.W. Cruse, A. Farooq, Y. Gultneh, R.R. Jacobson, N.J. Blackburn, R.W. Strange, J. Zubieta, J. Am. Chem. Soc. 110 (1988) 6769.
[71] P.P. Paul, Z. Tyeklár, R.R. Jacobson, K.D. Karlin, J. Am. Chem. Soc. 113 (1991) 5322.
[72] P. Ghosh, Z. Tyeklár, K.D. Karlin, R.R. Jacobson, J. Zubieta, J. Am. Chem. Soc. 109 (1987) 6889.
[73] M. Mahroof-Tahir, N.N. Murthy, K.D. Karlin, N.J. Blackburn, S.N. Shaikh, J. Zubieta, Inorg. Chem. 31 (1992) 3001.
[74] M. Mahroof-Tahir, K.D. Karlin, J. Am. Chem. Soc. 114 (1992) 7599.
[75] D.E. Root, M. Mahroof-Tahir, K.D. Karlin, E.I. Solomon, Inorg. Chem. 37 (1998) 4838.
[76] (a) R.R. Jacobson, Z. Tyeklár, A. Farooq, K.D. Karlin, S. Liu, J. Zubieta, J. Am. Chem. Soc. 110 (1988) 3690. (b) Z. Tyeklár, R.R. Jacobson, N. Wei, N.N. Murthy, J. Zubieta, K.D. Karlin, J. Am. Chem. Soc. 115 (1993) 2677.
[77] (a) J. Reim, B. Krebs, Angew. Chem. Ed. Int. Engl. 33 (1994) 1969. (b) J. Reim, R. Werner, W. Haase, B. Krebs, Chem. Eur. J. 4 (1998) 289.
[78] M.J. Baldwin, P.K. Ross, J.E. Pate, Z. Tyeklár, K.D. Karlin, E.I. Solomon, J. Am. Chem. Soc. 113 (1991) 8671.